



AIAA 99–2861

**The Far-Field Plasma Environment
of a Hollow Cathode Assembly**

Sven G. Bilén, Matthew T. Domonkos, and Alec D.
Gallimore

University of Michigan, Ann Arbor, Michigan 48109

**35th AIAA/ASME/SAE/ASEE Joint Propulsion
Conference and Exhibit**

20–24 June 1999

Los Angeles, California

The Far-Field Plasma Environment of a Hollow Cathode Assembly

Sven G. Bilén,^{*} Matthew T. Domonkos,[†] and Alec D. Gallimore[‡]
University of Michigan, Ann Arbor, Michigan 48109

Using a hollow cathode assembly (HCA) in a large vacuum chamber, such as the University of Michigan's Large Vacuum Test Facility (LVTF), provides the capability of generating a plasma environment that closely approximates that of the ionosphere. This capability allows examinations of ionospheric-plasma phenomena in a controlled setting without, in most cases, relying on scaling techniques. The HCA provides a low-temperature, low-density, fairly uniform plasma in its far-field, and the LVTF provides ample room such that the effects of plasma confinement can be reduced to a minimum. Most previous studies on the HCA have concentrated on its plasma environment in the near-field, *i.e.* within a few 10's of cm. This work, however, examines the far-field (*i.e.*, 1–2 m) plasma environment of the HCA. This characterization shows that the HCA provides, in the far-field, a fairly uniform ionospheric-level plasma environment. The HCA was operated at nine different operating conditions consisting of three different gases (argon, krypton, and xenon) each at three different flow rates. In this paper, results from these nine operating conditions are summarized and the corresponding far-field plasma environments are analyzed. Comparison of the HCA's plasma environment parameters with typical ionospheric values is presented.

Nomenclature

B_0	background magnetic-flux density, T
B_{LVTF}	magnetic-flux density in LVTF, T
\mathbf{B}_E	geomagnetic-flux-density vector, T
B_E	geomagnetic-flux density, T
\mathbf{B}_{IGRF}	magnetic-flux density from IGRF model, T
k	Boltzmann's constant, 1.38×10^{-23} J/K
m_e	electron mass, 9.109×10^{-31} kg
m_i	ion mass, kg
n_e	electron plasma density, m^{-3}
n_i	ion density, m^{-3}
q	charge magnitude, 1.602×10^{-19} C
r_{ce}	electron gyroradius, m
r_{ci}	ion gyroradius, m
T_e	electron temperature, K
v_{te}	electron thermal velocity, m/s
v_{ti}	ion thermal velocity, m/s
Z_i	ionization level, integer
ε_0	free space permittivity, 8.85×10^{-12} F/m
θ_e	electron temperature, eV

Introduction

THE capability of generating a plasma environment that closely approximates that of the ionosphere is highly desirable to researchers wishing to ex-

amine ionospheric-plasma phenomena in a controlled setting. Such a capability would also be useful in testing and calibrating ionospheric probes without relying on scaling techniques.¹ The use of a hollow cathode assembly (HCA) in a large vacuum chamber, such as the University of Michigan's Large Vacuum Test Facility (LVTF), can provide just such a capability. The HCA provides a low-temperature, low-density, fairly uniform plasma in its far-field, and the LVTF provides ample room such that the effects of plasma confinement—*i.e.*, interaction with the walls and support structures—can be reduced to a minimum.

The general operation of HCA's has been studied extensively in the literature.^{2–6} Many previous studies of the HCA have concentrated on its plasma environment in the near-field, *i.e.* within a few 10's of cm.^{6,7} Several works have also investigated the interaction of the HCA plume with an ambient plasma,^{8–11} although this is not the case of this study. Rather, this work examines the far-field (*i.e.*, ~1–2 m) plasma environment of the HCA. This characterization shows that the HCA provides, in the far-field, a fairly uniform ionospheric-level plasma environment.

The HCA was operated at a total of nine different operating conditions: three different gases (argon, krypton, and xenon), each at three different flow rates. In this paper, we begin by describing the vacuum chamber and experimental apparatus. We then present and summarize the results from the nine operating conditions and analyze the corresponding far-field plasma environments. We conclude by presenting an evaluation of our method and apparatus for simulating ionospheric plasmas.

^{*}Research Fellow, Radiation Laboratory and Space Physics Research Laboratory, AIAA Member

[†]NASA Graduate Student Researchers Program Fellow, Plasmadynamics and Electric Propulsion Laboratory, AIAA Student Member

[‡]Associate Professor, Aerospace Engineering and Applied Physics, AIAA Associate Fellow

Copyright © 1999 by Sven G. Bilén. Published by the American Institute of Aeronautics and Astronautics, Inc. with permission.

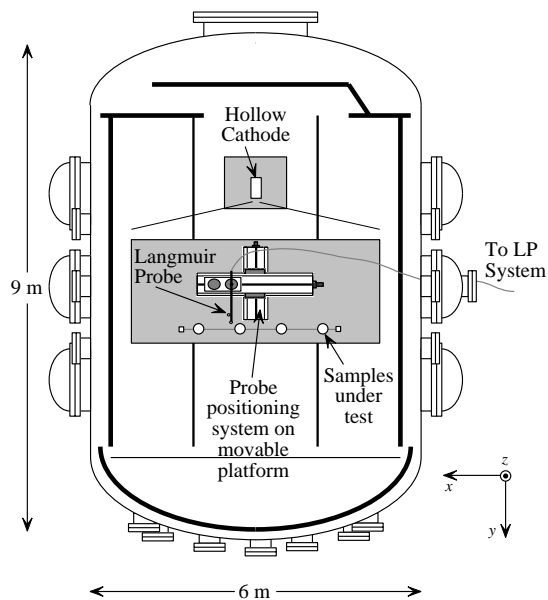


Fig. 1 Setup of the vacuum chamber for the far-field plasma environment characterization of the hollow cathode assembly (HCA) showing the location of the HCA and the Langmuir probe mounted on the positioning table. The items marked “Samples under test” are for a different set of experiments that the HCA characterization supported.

Experimental Apparatus

Vacuum Chamber Description

The University of Michigan’s Plasmadynamics and Electric Propulsion Laboratory (PEPL) has as its centerpiece the Large Vacuum Test Facility (LVTF), a cylindrical, stainless-steel-clad tank which is 9 m long and 6 m in diameter.¹² During these tests, the facility was supported by six 32,000 l/s diffusion pumps backed by two 2000 cfm (56,600 l/s) blowers and four 400 cfm (11,300 l/s) mechanical pumps. These pumps gave the facility an overall pumping speed of over 100,000 l/s on nitrogen and 25,000 l/s on xenon.[§] Fig. 1 is a diagram of the LVTF as it was set up for the HCA far-field plasma-environment characterization. It should be noted that these experiments provided background information for another set of experiments performed at the same time [see Bilén,¹³ Chap. 3].

The positioning table, also shown in Fig. 1, contains two rotary platforms on two transverse linear stages. This setup provides two degrees of freedom as well as angular freedom in the horizontal plane, *i.e.*, radial (x -plane), axial (y -plane), and θ . Altitude (z -plane)

[§]In Winter 1998, the LVTF underwent a major facilities upgrade during which four nude cryopumps were added. These cryopumps have a combined pumping speed of 300,000 l/s on air and 140,000 l/s on xenon and provide the ability to reach a high-vacuum (10^{-7} torr).

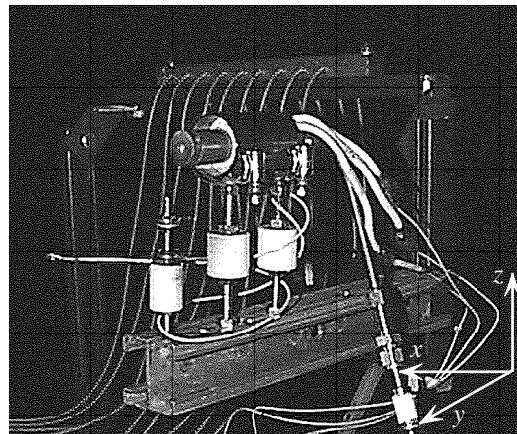


Fig. 2 Picture of the hollow cathode assembly as set up for these experiments (axis orientation shown in this figure corresponds to that of Fig. 1).

is fixed.[¶] The entire system is mounted on a movable platform allowing measurements to be made throughout a large portion of the chamber. The system can sweep two probes at a time at radial speeds in excess of 60 cm/s, with a positioning accuracy of 1 mm.

Hollow Cathode Assembly Description

The source for simulating the ionospheric plasma was a laboratory model hollow cathode assembly (HCA), which uses an orificed hollow cathode.¹⁴ The HCA was developed at NASA Glenn Research Center under its International Space Station plasma contactor program. The HCA created a low temperature plasma ($\theta_e \lesssim 1.5$ eV) by establishing a discharge between a hollow cathode chamber and a positive keeper electrode and was operated primarily in spot mode.¹⁵ Plasma density was varied by adjusting the flow rate. Fig. 2 shows a picture of the HCA as it looked during these tests. Table 1 gives a summary of the nine different HCA operating conditions.

Measurement Equipment

The measurement equipment used during the experiments included an electrometer, computer controller, magnetometer, and the aforementioned positioning table. The electrometer was connected via an IEEE-488 bus to a computer controller which set equipment parameters, controlled instruments, and stored data. A more detailed description of the equipment used and their function is listed below.

Electrometer A Keithley 2410 Source Electrometer was used to drive the Langmuir probe (LP) system. The electrometer measured the current collected by the LP as it was swept from -20 to 20 V. The LP was positioned via the positioning table. LP measurements were used to determine

[¶]Recently, the capability for z -axis motion has been added to the positioning table.

Table 1 Summary of the operating conditions of the hollow cathode assembly.

Oper. Cond.	Gas	Flowrate, sccm	Discharge Voltage, V	Discharge Current, A	Mode of Operation	Tank Pressure, $\times 10^{-5}$ torr (indicated)
1	krypton	10.2	14.8	3.97	spot	4.9
2	krypton	19.2	14.8	3.97	spot	4.9
3	krypton	4.3	19.3	3.97	plume	4.9
4	argon	12.9	17.2	3.97	spot	4.9
5	argon	18.3	15.8	3.97	spot	5.2
6	argon	14.8	16.5	3.97	spot	5.1
7	xenon	2.3	15.5	3.97	transition	4.5
8	xenon	6.9	14.8	3.97	spot	5.2
9	xenon	3.9	17.1	3.97	transition	4.8

electron temperatures and number densities of the HCA plasma plume.

Computer Controller An Apple Macintosh Quadra running LabVIEW software from National Instruments was used to set equipment parameters and to store data via an IEEE-488 bus. LabVIEW routines were used to drive the electrometer and capture LP traces.

Positioning Table The positioning table, developed by New England Affiliated Technologies (NEAT), was used to position the LP throughout the far-field region of the HCA plume.

Magnetometer The Shuttle Electrodynamic Tether System¹⁶ (SETS) aspect magnetometer (AMAG) was used to determine the orientation and strength of the geomagnetic field present in the plasma chamber. This instrument provides three-axes absolute-field measurements with 468-nT resolution.^{||}

Langmuir Probe Measurement Positions

The Langmuir probe measurements were made at 12 locations throughout the chamber for each of the nine HCA operating conditions. The 12 locations are shown in Fig. 3. The measurement space covers an area of about 1.4 m \times 0.7 m, with the closest measurement made about 1.2 m away from the HCA. The measurement space is oriented fairly symmetrically about the axis of the HCA plume. The location of the HCA is at the (0,0) point of Fig. 3.

Experimental Results

Electron Densities

The electron density throughout the measurement region was determined via the Langmuir probe method as outlined in Krehbiel et al.¹⁷ The LP bias voltage was swept from -20 to +20 V in 200 steps and the resulting current was measured via the electrometer. The rhenium LP tip was cylindrically shaped, 48.9 mm

^{||}The SETS instrument data was collected during a previous set of experiments; the instrument was not in the LVTF during this experiment.

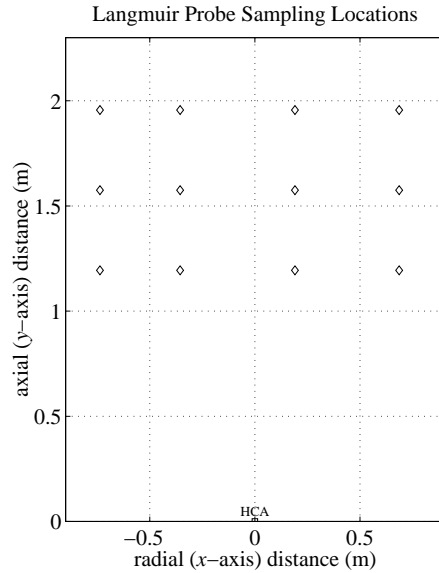


Fig. 3 Locations of the Langmuir probe measurements with respect to the hollow cathode assembly.

long with a diameter of 3.9 mm, and was mounted on a triaxial mast to ensure that the low ion currents could be measured. The probe is very similar to those used on previous ionospheric missions such as *Dynamics Explorer*. The probe was periodically cleaned using electron bombardment of its surface by applying +200 V to the probe tip. A typical I-V characteristic from this experiment is shown in Fig. 4.

Using the n_e values obtained through analysis of the LP data, contour plots of n_e throughout the measurement region were produced for each of the nine HCA operating conditions (see Table 1). A cubic interpolation of the data collected at the 12 locations provides a smooth estimate of n_e throughout the measurement region. The plots in Figs. 5–13 show the electron density in the HCA plume for each of the nine operating conditions. Table 2 gives a summary of the plasma environment as measured by the LP.

There are some items to note in the data presented in Figs. 5–13. First, most of the plots appear to have slighter higher densities to the right of the HCA. It

Table 2 Summary of the plasma environment from the hollow cathode assembly for each of the nine operating conditions.

Oper. Cond.	Gas	Ion Mass, $\times 10^{-26}$ kg	Mean n_e (std. dev.), $\times 10^{12}$ m^{-3}	Mean θ_e (std. dev.), eV	Fig. Num.
1	krypton	13.92	3.9 (0.9)	0.9 (0.1)	5
2	krypton	13.92	11.9 (3.3)	1.1 (0.3)	6
3	krypton	13.92	1.2 (0.3)	1.0 (0.2)	7
4	argon	6.63	1.2 (0.1)	1.0 (0.2)	8
5	argon	6.63	1.5 (0.2)	1.1 (0.3)	9
6	argon	6.63	1.0 (0.1)	1.8 (0.2)	10
7	xenon	21.80	1.6 (0.3)	1.5 (0.1)	11
8	xenon	21.80	7.5 (1.7)	1.4 (0.1)	12
9	xenon	21.80	2.9 (0.4)	1.5 (0.1)	13

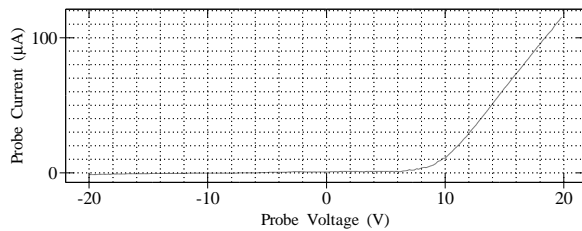


Fig. 4 A sample current–voltage characteristic for the cylindrical Langmuir probe used in this experiment (data is from Condition 7, sample 2, point closest to the HCA—see Figure 11).

is believed that this was due to the HCA pointing slightly to the right of the center line. Second, although the region is undersampled, fairly good density profiles can be interpolated due to the uniform nature of the plasma plume.

Ion Densities

The ion density throughout the measurement region was determined via the Langmuir probe method. These values were all within a factor of 2 of the electron densities providing important corroboration of the results.

Electron Temperatures

The electron temperature throughout the measurement region was determined via the Langmuir probe method. These values fell within the range 0.9 to 1.8 eV.

Chamber Ambient Magnetic Field

The ambient magnetic field in the chamber was measured with the SETS AMAG during thermal-vacuum testing of the SETS payload on 2 February 1995. The AMAG-measured magnetic field is $\mathbf{B}_{LVTF} = -1.83\hat{x} + 7.86\hat{y} - 4.26\hat{z} \times 10^3$ nT or $|\mathbf{B}_{LVTF}| = 9.12 \times 10^3$ nT (coordinates are those shown in Figure 1). Such a low value for the ambient LVTF magnetic field may at first seem incorrect since the International Geomagnetic Reference Field (IGRF) model¹⁸ predicts a value

of $|\mathbf{B}_{IGRF}| = 5.63 \times 10^4$ nT.* However, the LVTF is made of both stainless steel, which is generally non-magnetic,¹⁹ and ferrous steel components. The ferrous components of the LVTF affect the local field, in this case greatly reducing it. Thus, the reduction in field strength observed inside the LVTF can be explained.

Discussion

The data collected during this experiment and analyzed here show that the far-field plasma environment of the HCA approximates that of ionospheric plasmas. Table 3 compares typical values for several ionospheric parameters with those provided by the HCA in the LVTF. We discuss these and other parameters in the remainder of this section.

Plasma Density and Confinement

This characterization effort showed that the obtainable density range from the HCA in the LVTF is between $\sim 10^{12}$ to 10^{13} m^{-3} and higher. This range adequately covers the higher plasma densities found in the ionosphere during daytime and/or solar maximum, but is higher than those found during nighttime and/or solar minimum (as low as $\sim 10^{10}$ m^{-3}). However, lower densities ($\sim 10^{11}$) can be obtained in the LVTF farther back from the HCA than this study's measurement space.

One very important aspect of the HCA's plasma environment is that the plasma is uniform over a fairly large region (1–2 m). Density and electron temperature vary by only $\lesssim 2$ from side to side and front to back of the measurement space used in this study. In addition, the LVTF's walls are located a large distance from the plasma region of interest, minimizing the confining effects of the walls—often one of the largest problems with simulating an ionospheric plasma. These two aspects allow large and/or distributed systems to be placed in the plasma without requiring compensation for changing conditions across

*The location of the chamber is 42°17'98.41" N lat., 83°41'61.98" E long. For this location, IGRF predicts an ambient geomagnetic field of $\mathbf{B}_{IGRF} = 1.83\hat{x} - 0.19\hat{y} + 5.32\hat{z} \times 10^4$ nT, where \hat{x} is directed North, \hat{y} is directed East, and \hat{z} is directed into the Earth.

Table 3 Comparison of a typical ionospheric plasma environment with that provided by the hollow cathode assembly in the Large Vacuum Test Facility.

Parameter	Typical Ionospheric Value	Chamber Value	Comments
n_e	10^{10} – 10^{13} m ⁻³	10^{11} – 10^{13} m ⁻³	depends on distance from HCA and gas flowrate
T_e (θ_e)	1160–3480 K (0.1–0.3 eV)	10400–23100 K (0.9–2.0 eV)	lower possibly with cold gas injection at HCA keeper
m_i (O ⁺)	2.66×10^{-26} kg	$\in [6.63, 13.92, 21.80] \times 10^{-26}$ kg	other gases available, <i>e.g.</i> , neon (3.35×10^{-26} kg)
B_E	35000 nT (0.35 G)	~ 9000 nT	auxiliary field can be added with Helmholtz coils

the system. In addition, these aspects allow for the examination of large sheaths, *e.g.*, on high-voltage conductors.¹³

Electron Temperature

The electron temperatures obtained in the study were in the range of $\simeq 0.9$ to 1.8 eV. These values are slightly higher than those found in the ionosphere ($\theta_e \simeq 0.1$ to 0.3 eV), but not appreciably so. Electron temperature could possibly be lowered in future experiments by injecting cold gas at the exit of the HCA keeper or by adding polyatomic molecules such as nitrogen to the noble gas HCA propellant. By running a small HCA in spot mode²⁰ it may also be possible to achieve lower electron temperatures.

Primary Ion Constituent

The three gases used here—argon, krypton, and xenon—are all heavier than the primary ionospheric constituent: atomic oxygen. In our study, we did attempt to use neon, which is close in mass to oxygen, but the cathode ran hot at the low flowrate required to achieve low densities. For this reason, higher flowrates were required but they produced a much denser plasma than ionospheric levels at 1–2 m from the HCA exit plane. It may be possible to modify the orifice such that the lower flowrates do not overheat the cathode allowing better ion mass matching with neon in future experiments.

Magnetic Field

Knowledge of the ambient magnetic field found in the ionosphere and the LVTF is important because it affects several plasma scale lengths and resonance frequencies. The geomagnetic field strength measured in the chamber is about a factor of four smaller than that in the ionosphere. This, however, is not necessarily disadvantageous since the addition of Helmholtz coils would allow for varying magnetic field orientations without much interference from the ambient geomagnetic field. For future experiments requiring ambient magnetic fields, we are investigating the possibility of adding Helmholtz coils to the LVTF.

Resonance Frequencies and Scale Lengths

Often what is most important in the experimental simulation of ionospheric plasma is how closely the plasma resonance frequencies and scale lengths are approximated. Resonance frequencies of interest include the electron and ion plasma frequencies, ω_{pe} and ω_{pi} ; the electron and ion cyclotron frequencies, ω_{ce} and ω_{ci} ; and the upper and lower hybrid frequencies, ω_{uh} and ω_{lh} . Scalelengths of interest include the Debye length, λ_D , and the electron and ion cyclotron radii, r_{ce} and r_{ci} .[†] Table 4 summarizes these parameters and gives equations for their derivation along with values for a typical ionosphere and the HCA far field.

By examining the equations for the frequencies and scale lengths given in Table 4 we can determine how closely the values in the HCA plasma environment will approximate those of the ionosphere. In general, the HCA’s far-field plasma is good for simulating electron dynamics, but less so for ions. For example, because ω_{pe} depends only on n_e , this frequency can be matched closely. Other frequencies that depend on m_i and/or B_0 are not matched as closely, but are still reasonably close. With respect to scale length, we see that the electron gyroradius is easily contained within the plasma environment, whereas the ion gyroradius is clearly not contained. Finally, because the important λ_D scale length is proportional to $\sqrt{T_e/n_e}$, it can be matched very closely.

Nonidealities

Although there are many properties of ionospheric plasma that the far-field of the HCA approximates, there are several properties which do deviate significantly from ionospheric plasmas. Besides the deviations in ion mass and magnetic-field strength noted above, there is another deviation that has to do with plasma flow. Most *in situ* investigations in the ionosphere are connected to moving spacecraft with orbital velocities high enough that the ion flow is effectively a directed beam. The HCA does not provide such a

[†]In the calculations of r_{ce} and r_{ci} , we define thermal velocities as $v_{tj} = \sqrt{kT_j/m_j}$, for $j = e, i$ and let $T_e = T_i$.

Table 4 Table summarizing typical ionospheric and far-field HCA parameters using parameter ranges found in Table 3.

Parameter	Equation	Typical Ionospheric Values	Chamber Range
ω_{pe}	$\sqrt{\frac{n_e q^2}{\epsilon_0 m_e}}$	5.64–178 Mrad/s (0.898–28.4 MHz)	17.8–178 Mrad/s (2.84–28.4 MHz)
ω_{pi}	$\sqrt{\frac{n_i Z_i^2 q^2}{\epsilon_0 m_i}}$	32.9–1040 krad/s (5.23–165 kHz)	Xe:36.5–Ar:661 krad/s (5.80–105 kHz)
ω_{ce}	$\frac{qB_0}{m_e}$	6.16 Mrad/s (908 kHz)	1.58 Mrad/s (252 kHz)
ω_{ci}	$\frac{Z_i q B_0}{m_i}$	209 rad/s (33.3 Hz)	Xe:6.6 rad/s (1.1 Hz), Ar:22 rad/s (3.5 Hz)
ω_{uh}	$\sqrt{\omega_{pe}^2 + \omega_{ce}^2}$	8.35–178 Mrad/s (1.33–28.4 MHz)	17.9–178 Mrad/s (2.84–28.4 MHz)
ω_{lh}	$\approx \sqrt{\omega_{ce}\omega_{ci}}$	35.9 krad/s (5.71 kHz)	5.9 krad/s (938 Hz)
λ_D	$\sqrt{\frac{\epsilon_0 k T_e}{q^2 n_e}}$	0.75 mm–4.1 cm	2.2 mm–3.3 cm
r_{ce}	$\frac{m_e v_{e,\perp}}{qB} = \frac{v_{te}}{\omega_{ce}}$	2.15–3.73 cm	25–37 cm
r_{ci}	$\frac{m_i v_{i,\perp}}{qB} = \frac{v_{ti}}{\omega_{ci}}$	3.71–6.43 m	Ar:67–100 m

directed flow, and hence motional effects cannot be readily studied with the HCA in the LVTF.

Summary

The capability of generating a plasma environment that closely approximates the ionosphere’s is useful for examining ionospheric-plasma phenomena in a controlled setting. The data collected and analyzed in this study show that the far-field plasma environment of the HCA approximates ionospheric plasmas. The obtainable density range during this study was between $\sim 10^{12}$ to 10^{13} m^{-3} and higher, but if tests are performed farther back in the LVTF, lower densities ($\sim 10^{11}$) can be obtained. The electron temperatures were in the range of $\simeq 0.9$ to 1.8 eV. The plasma is fairly uniform over a large region, varying by only a factor of 2 from side to side and front to back of the measurement space used in this study.

Acknowledgments

The authors wish to thank Michael Patterson of NASA Glenn Research Center for the loan of the HCA used in this research. In addition, the authors wish to thank the PEPL research group and Preston Powell, a 1997 Summer Research Experience for Undergraduates (REU) student, for help with the Langmuir probe analyses.

References

¹Smith, J., “Low Density Plasma Generation and Measurement” (abstract), *EOS, Transactions, American Geophysical Union*, Vol. 51, No. 11, 1970, p. 785.
²Mavrodineanu, R., “Hollow Cathode Discharges,” *Journal of Research of the National Bureau of Standards*, Vol. 89, No. 2, 1984, pp. 143–185.
³Parks, D. E., Mandell, M. J., and Katz, I., “Fluid Model of Plasma Outside a Hollow Cathode Neutralizer,” *Journal of Spacecraft and Rockets*, Vol. 19, No. 4, 1982, pp. 354–357.
⁴Gerver, M. J., Hastings, D. E., and Oberhardt, M. R., “Theory of Plasma Contactors in Ground-Based Experiments and Low Earth Orbit,” *Journal of Spacecraft and Rockets*, Vol. 27, No. 4, 1990, pp. 391–402.

⁵Parks, D. E., Katz, I., Buchholtz, B., and Wilbur, P., “Expansion and Electron Emission Characteristics of a Hollow-Cathode Plasma Contactor,” *Journal of Applied Physics*, Vol. 74, No. 12, 1993, pp. 7094–7100.
⁶Conde, L., León, L., and Ibáñez, L. F., “Electron Transport Properties of Stationary Plasma Clouds Generated with Hollow Cathode Discharges,” *IEEE Transactions on Plasma Science*, Vol. PS-25, No. 4, 1997, pp. 548–552.
⁷Williams, J. D., and Wilbur, P. J., “Experimental Study of Plasma Contactor Phenomena,” *Journal of Spacecraft and Rockets*, Vol. 27, No. 6, 1990, p. 634–641.
⁸Hastings, D. E., “Theory of Plasma Contactors Used in the Ionosphere,” *Journal of Spacecraft and Rockets*, Vol. 24, No. 3, 1987, pp. 250–256.
⁹Parks, D. E., and Katz, I., “Theory of Plasma Contactors for Electrodynamic Tethered Satellite Systems,” *Journal of Spacecraft and Rockets*, Vol. 24, No. 3, 1987, pp. 245–249.
¹⁰Iess, L., and Dobrowolny, M., “The Interaction of a Hollow Cathode with the Ionosphere,” *Physics of Fluids B*, Vol. 1, No. 9, 1989, pp. 1880–1889.
¹¹Vannaroni, G., Dobrowolny, M., Melchioni, E., Venuto, F. D., and Giovi, R., “Characterization of the Interaction Between a Hollow Cathode Source and an Ambient Plasma,” *Journal of Applied Physics*, Vol. 71, No. 10, 1992, pp. 4709–4717.
¹²Gallimore, A. D., Kim, S.-W., Foster, J. E., King, L. B., and Gulczinski III, F. S., “Near and Far Field Plume Studies of a One-Kilowatt Arcjet,” *AIAA J. Prop. Power*, Vol. 12, 1996, pp. 105–111.
¹³Bilén, S. G., “Pulse Propagation Along Conductors in Low-Density, Cold Plasmas as Applied to Electrodynamic Tethers in the Ionosphere,” Ph.D. thesis, 332 pp., Univ. of Michigan, 1998.
¹⁴Sarver–Verhey, T. R., “Continuing Life Test of a Xenon Hollow Cathode for a Space Plasma Contactor,” NASA CR–195401, Nov. 1994.
¹⁵Rawlin, V. K., and Pawlik, E. V., “Mercury Plasma-Bridge Neutralizer,” *Journal of Spacecraft and Rockets*, Vol. 5, No. 7, 1968, pp. 814–820.
¹⁶Agüero, V., Banks, P. M., Gilchrist, B., Linscott, I., Raitt, W. J., Thompson, D., Tolat, V., White, A. B., Williams, S., and Williamson, P. R., “The Shuttle Electrodynamic Tether System (SETS) on TSS-1,” *Il Nuovo Cimento*, Vol. 17C, No. 1, 1994, pp. 49–65.
¹⁷Krehbiel, J. P., Brace, L. H., Theis, R. F., Pinkus, W. H., and Kaplan, R. B., “The Dynamics Explorer Langmuir Probe Instrument,” *Space Science Instrumentation*, Vol. 5, 1981, pp. 493–502.
¹⁸Barton, C. E., “International Geomagnetic Reference

Field: The Seventh Generation," *Journal of Geomagnetism and Geoelectricity*, Vol. 49, No. 2-3, 1997, pp. 123-148.

¹⁹Bozorth, R. M., *Ferromagnetism*, D. Van Nostrand Company, New York, NY, 1951.

²⁰Domonkos, M. T., Gallimore, A. D., and Patterson, M. J., "Low-Current Hollow Cathode Evaluation," AIAA Paper No. 99-2575, 35th AIAA/ASME/SAE/ASEE Joint Propulsion Conference, June 1999, Los Angeles, CA.

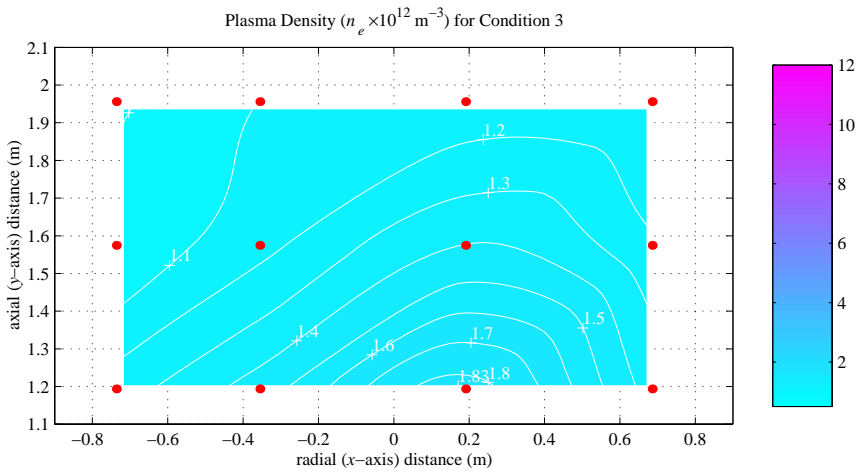
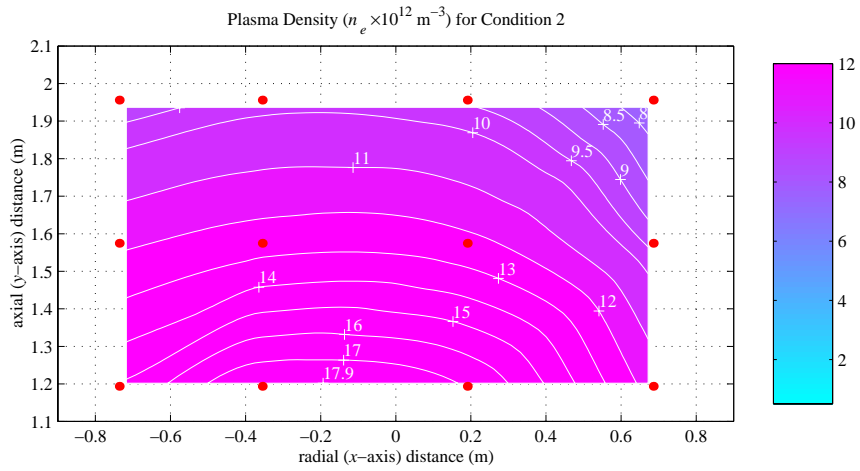
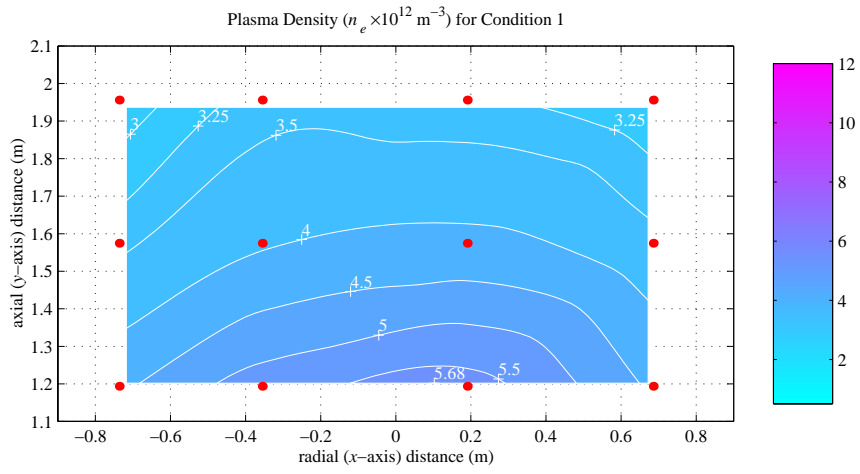


Fig. 7 Spatial distribution of electron density for Condition 3.

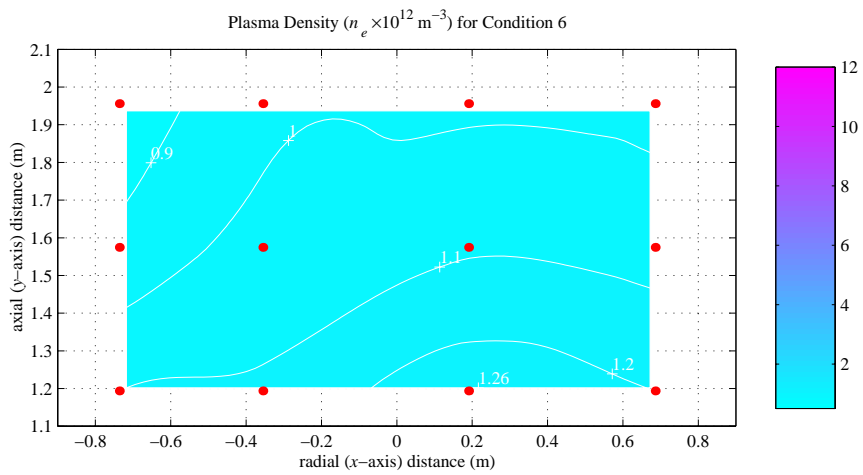
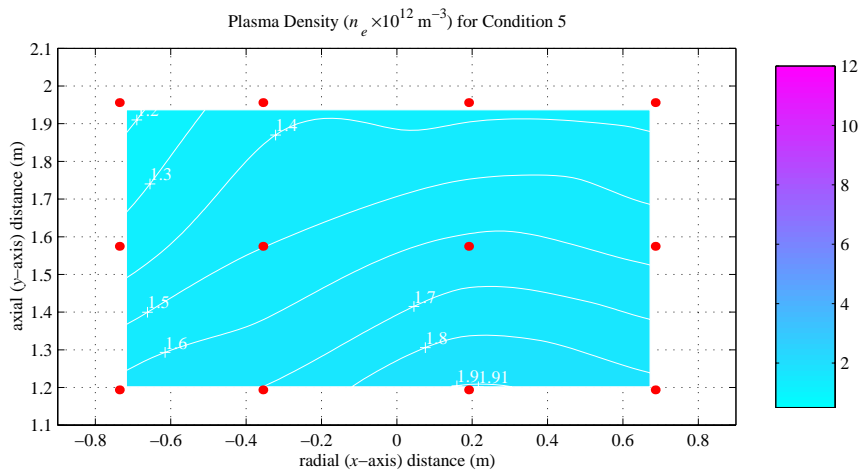
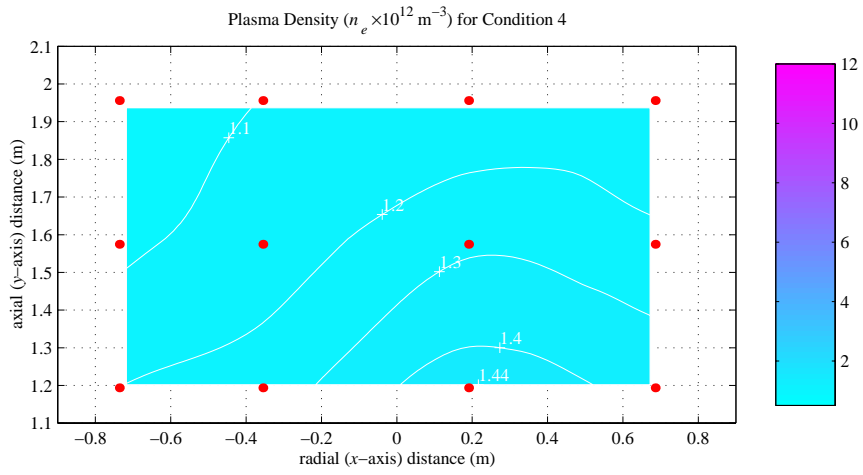


Fig. 10 Spatial distribution of electron density for Condition 6.

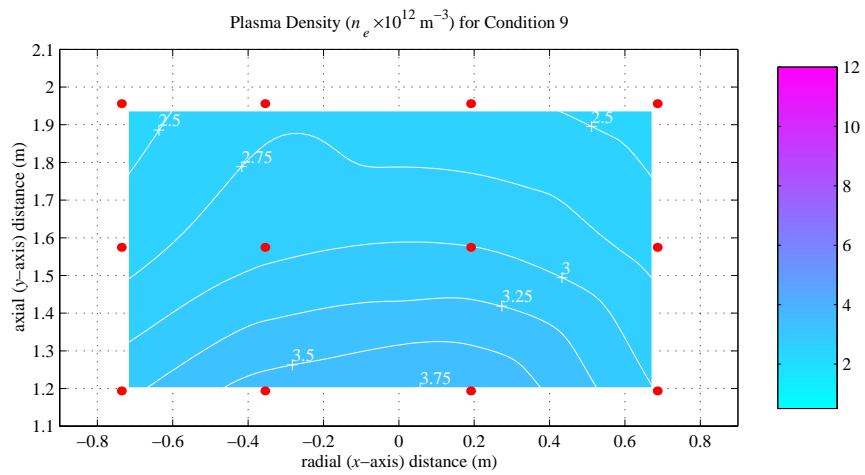
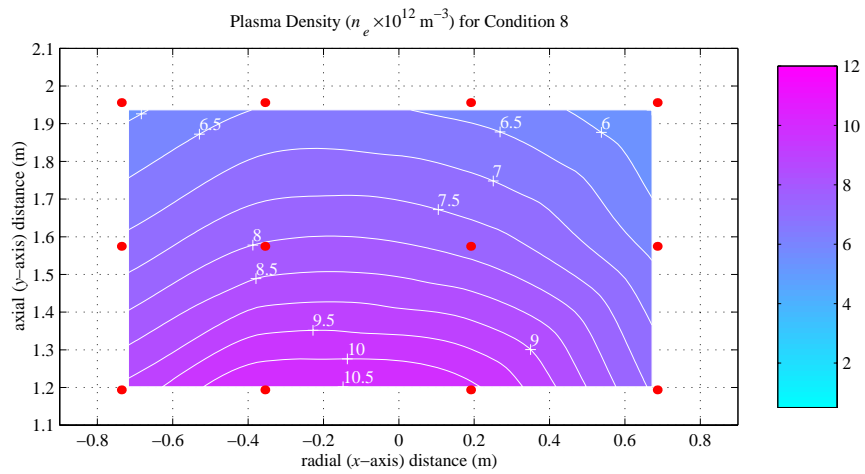
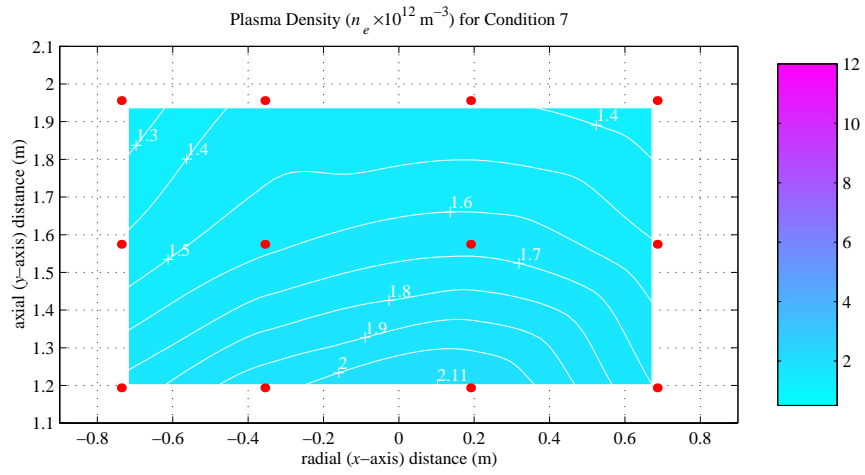


Fig. 13 Spatial distribution of electron density for Condition 9.